Clays and Clay Minerals, Vol. 67, No. 4:253–264, 2019

PHOTOCATALYTIC ACTIVITY OF La-CONTAINING MIXED-METAL OXIDES DERIVED FROM LAYERED DOUBLE HYDROXIDES TO DEGRADE METHYLENE BLUE IN THE PRESENCE OF H_2O_2

Minhong Xu[1] *, Mengxia Qian[2], Guoxiang Pan[1], Yuhua Guo[1], and Tao Wu[1]

[1]Department of Materials Engineering, Huzhou University, Huzhou 313000, China
[2]Key Laboratory of Advanced Textile Materials and Manufacturing Technology of Ministry of Education, Zhejiang Sci-Tech University, Hangzhou 310018, China

Abstract—Photocatalytic degradation of polluted water by means of minerals, such as clays and oxides, which have surfaces that exhibit catalytic properties, has been suggested to be a useful new strategy to promote both organic and inorganic pollutant degradation. Nevertheless, much still remains to be studied about the capability of mixed metal oxides derived from lanthanum-containing layered double hydroxides to promote pollutant removal by means of photocatalytic degradation with the mineral surfaces. The objective of the present study was to investigate the synthesis of ternary MgAlLa mixed-metal oxides (MgAlLa-M) with various Mg/Al/La molar ratios through a hydrotalcite-like precursor route by co-precipitation of appropriate amounts of metal salts from homogeneous solution, followed by calcination at 600°C. The crystal structure, surface morphology, and optical properties of the samples were characterized by X-ray diffraction (XRD), scanning electron microscopy (SEM), Fourier-transform infrared spectroscopy (FTIR), and UV-Vis diffuse reflectance spectroscopy (DRS). Analysis by XRD showed that MgO, La_2O_3, $MgAl_2O_4$, and $La_{10}Al_4O_{21}$ phases coexisted in calcined samples as MgAlLa-M. The samples showed a small band gap of 3.11 3.35 eV according to DRS. The photocatalytic activities of the samples were evaluated by degradation of methylene blue (MB) under visible light irradiation. MgAlLa-M had better photocatalytic properties than hydrotalcite precursors, and the MgAlLa-0.5-M possessed the best photocatalytic activity. The photocatalytic degradation efficiency of MB dye with MgAlLa-0.5-M under visible light irradiation for 1 h was 99.89% in the presence of H_2O_2, which exceeded the binary MgAl-M (84.06%) under the same conditions. The high photocatalytic activity of the sample was attributed to the addition of La(III). In addition, the possible mechanism of photocatalytic degradation of MB by MgAlLa-M was discussed. The results showed that O_2^- plays a major role in the MgAlLa-0.5-M/H_2O_2 system.

Keywords—Co-precipitation method · Hydrotalcites · Methylene Blue · Mixed metal oxides · Photocatalytic activity

INTRODUCTION

The pollution of water by organic contaminants, such as Methylene Blue (MB), is a serious problem because of high toxicity and persistence in the environment (Ömer et al. 2015). The efficient removal of organic dyestuffs from industrial polluted water has always been a challenging issue in the field of environmental remediation and pollution control (Li et al. 2017; Kong et al. 2018). The removal of a binary dye mixture of Congo Red and Malachite Green from aqueous solutions using a bentonite adsorbent was proposed by Özdemir & Keskin (2009). Moreover, photocatalysts with semiconductor properties are considered important in such key remediation processes as water photolysis, photodegradation, photooxidation of toxic compounds, and photoelectrochemical conversion (Carja et al., 2013; Xu et al. 2019), where they act as efficient eco-friendly materials for removal of hazardous species.

Layered double hydroxides (LDHs) or hydrotalcite-like materials belong to a family of anionic clays with a brucite-like layered structure (Zhou 2010; Zhou & Keeling 2013). Compared with synthetic clay minerals, LDHs have a wider range of chemical compositions of layers based on different choices of metal and interlayer anions (Shi et al. 2005; Curtius and Ufer 2007; Zhou et al. 2016). Thus, LDHs are well known for their catalytic activity in organic synthesis (Shu et al. 2008; Xiang et al. 2008; Zhou 2010). LDHs are also ideal precursors for obtaining various mixed-metal oxides possessing tunable compositions upon heating (Xiang et al. 2008). Furthermore, calcination of LDH materials at moderate temperatures (300 600°C) leads to the formation of highly active mixed-metal oxide (MMO) nanocomposites with large specific surface areas and good thermal stability, which can tune the semiconductor properties of the MMO materials and facilitate the transfer of the photogenerated electrons to the surface of photocatalysts. In particular, the mixed-metal oxides prepared by thermal treatment of LDHs act as photocatalysts either for organic degradation or for water splitting, and have been the focus of attention due to their versatility of chemical

* E-mail address of corresponding author: xumh123@163.com
DOI: 10.1007/s42860-019-00023-2

This paper was originally presented during the World Forum on Industrial Minerals, held in Qing Yang, China, October 2018.

composition and wide dispersion (Parida et al. 2012; Baliarsingh et al. 2013; Wu et al. 2014). The effect of Cu substitution on promoted benzene oxidation over porous CuCo-based catalysts derived from LDH was discussed by Li et al. (2015). A maximum of 97.3% photocatalytic decoloration rate within 60 min was achieved from the LDHs with a Zn/Ni/Al mole ratio of 2:1:1 and calcination temperature of 500°C according to Li et al. (2017). A 150 W xenon lamp with λ = 200 −900 nm was used as the simulated sunlight source. Calcined samples with a Ni/Co/Fe molar ratio of 1:2:1, derived from NiCoFe Ternary LDHs, possessed the best photocatalytic activity with 96.8% degradation of MB dye under Xenon lamp irradiation for 4 h, as reported by Pan et al. (2018). Although the photocatalytic effect was greater, the illumination time was longer. In addition, calcined ZnAlTi (Sahu et al. 2013), CoMgAl (Yang et al. 2017), and Mg-Al-Fe LDHs (Heredia et al. 2013) were reported. Moreover, the introduction of basic rare earth elements (La, Ce, or Y) into these materials can modify the basic sites and, thus, modulate the basicity of the catalyst (Wang et al. 2014; Subhan et al. 2015).

The rare earth elements (REE) have the characteristics of oxygen storage functionality, rapidly variable valence states, and so on. Furthermore, the rare earth oxides with cation valence, paramagnetic behavior, lattice oxygen transfer, and alkaline surfaces have properties related intrinsically to many catalytic activities. The precursor with large photocatalytic activity can be prepared by introducing rare earth elements into LDH. For the above reasons, rare earth elements were introduced into ternary hydrotalcite to make composite oxides. Ternary LDH precursors have been reported, configured with Mg-Al-Tb, Mg-Al-Eu, Zn-Al-In, Zn-In (ZnIn-LDH), or melamine mixtures. Ternary MgO/ZnO/In_2O_3 heterostructured photocatalysts derived from a layered precursor, MgFeCe ternary LDH, and Ce- and Pr-promoted Ni and Co catalysts from hydrotalcite-type precursors (Chen et al. 2011; Fan et al. 2011; Muñoz et al. 2012; Carja et al. 2013; Lan et al. 2014; Chen et al. 2015; Nivangune et al. 2017) have also been reported. Few reports, however, have appeared on La-containing composite oxides derived from ternary LDHs. With practical application in mind, therefore, efficient use of Earth-abundant metal elements (e.g. Mg) for synthesis of high-performance photocatalysts (Xiang et al. 2013) and broadening the use of rare metal elements (e.g. La) are of great signficance.

The purpose of the present study was to synthesize a series of ternary MgAlLa MMOs (MgAlLa-M) with various Mg/Al/La ratios and to test their photocatalytic performance in abating organic pollutants by measuring the degradation of MB in aqueous solution under visible irradiation. This study was also undertaken with the hope of broadening the field of utilization of rare earth resources in China by making full use of the exchangeability of cations on hydrotalcite laminates (Mao et al. 2017) and exploiting the high photocatalytic activity of REE.

EXPERIMENTAL

Materials

For this work, $Mg(NO_3)_2{\cdot}6H_2O$, $La(NO_3)_3{\cdot}6H_2O$, $Al(NO_3)_3{\cdot}9H_2O$, $NaNO_3$, NaOH, isopropanol, p-benzoquinone, ethylene diamine tetraacetic acid disodium salt, H_2O_2, and MB of analytical purity grade were purchased from Aladdin Reagent Co., Ltd (Shanghai, China). All solutions were prepared with distilled water.

Synthesis of MgAlLa-LDHs

A series of MgAlLa-LDHs with various molar ratios of Al(III)/La(III) were synthesized by the co-precipitation method. At a molar ratio M(II)/M(III) of 3.0, specific quantities of $Mg(NO_3)_2{\cdot}6H_2O$, $Al(NO_3)_3{\cdot}9H_2O$, and $La(NO_3)_3{\cdot}6H_2O$ solid were dissolved in distilled water, as solution A. Then NaOH and $NaNO_3$ were dissolved in distilled water; this was marked as solution B. With constant stirring, solutions A and B were added dropwise into a beaker, which was filled with distilled water. In this process, the mixed solution was adjusted with NaOH solution until the pH was between 9 and 10, after which the solution was stirred continuously for a further 30 min. Finally, the slurry obtained was subsequently aged at 65°C for 24 h. The resulting precipitates were collected by centrifugal separation and washed thoroughly with distilled water. After that, the as-obtained solid was oven-dried at 60°C overnight to obtain MgAlLa-LDHs precursors with various Mg(II)/Al(III)/La(III) (Mg/Al/La) molar ratios (i.e. 3:1:0, 3:0.8:0.2, 3:0.6:0.4, 3:0.5:0.5, 3:0.2:0.8, and 3:0:1); these precursors were denoted as MgAlLa-*x*-L, where *x* stands for the La(III) molar ratio. For example, the precursor with a Mg(II)/Al(III)/La(III) molar ratio of 3:1:0 was denoted as MgAl-L, that with a Mg(II)/Al(III)/La(III) molar ratio of 3:0.5:0.5 was specifically denoted as MgAlLa-0.5-L, and that with a Mg(II)/Al(III)/La(III) molar ratio of 3:0:1 was specifically denoted as MgLa-1-L.

Synthesis of mixed-metal oxides

The MgAlLa-LDH precursor was calcined in air at 600°C for 5 h, and allowed to cool to room temperature to obtain Mg/Al/La mixed-metal oxides, which were named MgAlLa-M. The mole ratios of Mg(II)/Al(III)/La(III) were 3:1:0, 3:0.8:0.2, 3:0.6:0.4, 3:0.5:0.5, 3:0.2:0.8, and 3:0:1, respectively. In the present study, the mixed-metal oxide with a Mg(II)/Al(III)/La(III) mole ratio of 3:0.8:0.2 was denoted specifically as MgAlLa-0.2-M.

Characterizations

The morphology of the samples was examined using a S-3400N scanning electron microscope (Hitachi, Tokyo, Japan). Elemental analysis was obtained using a Model 550i, energy dispersive X-ray fluorescence (EDX) (Model 550i, IXRF System, Austin, Texas, USA). The crystal phases in the samples were identified by XRD (CuKα, λ = 0.1545 nm, beam voltage 36 kV, beam current 20 mA) (Beijing Purkinje General Instrument Co., Ltd., Beijing, China). Infrared (FTIR) spectra were recorded using the KBr disc method on a Nicolet 5700 FTIR spectrophotometer (Thermo Scientific, Waltham, Massachusetts, USA). The sample was dried at 120°C for 1 h and then the

https://doi.org/10.1007/s42860-019-00023-2 Published online by Cambridge University Press

sample was mixed with KBr at a mass ratio of 1:100 for grinding and finally pressed into thin sheets for measurement. UV-Vis diffuse reflectance spectra (DRS) of the samples were obtained using an ISA-220 UV-Vis spectrophotometer (Thermo Scientific, Waltham, Massachusetts, USA). The time-dependent UV-Vis spectra of MB solutions were measured using a UV-2600 UV-vis spectrophotometer (Shimadzu, Tokyo, Japan).

Photocatalysis

The photocatalytic activities of the samples were assessed by photodegradation of MB solution under visible light irradiation from a 150 W halogen lamp, which was preheated for 30 min. Photocatalyst (0.05 g) was mixed with 25 mL of MB (5 mg/L) aqueous solution, to which was added 0.5 mL of H_2O_2 (30% w/w). For each run, 0.05 g of catalyst was added to a 25 mL MB solution and stirred vigorously for 30 min in the dark to establish an adsorption/desorption equilibrium. Subsequently, the solution was stirred under visible light irradiation. The catalyst was kept suspended by a magnetic stirrer. Samples for analysis were extracted using a pipette every 10 min and centrifuged immediately. After that, the filtrates were tested by measuring the absorbance at 664 nm using 752 UV-Vis spectroscopy to determine the concentration of MB. The effects of light and the La(III) content on the catalytic degradation of MB were investigated. Blank experiments, *i.e.* without catalyst or in the dark, were carried out under the same conditions.

RESULTS AND DISCUSSION

X-ray Diffraction

The powder XRD patterns of as-synthesized MgAlLa-L precursors with variable Mg(II)/Al(III)/La(III) molar ratios (Fig. 1) revealed that, as for the MgAl-L sample (Fig. 1a), the diffraction peaks at 11.7, 22.5, 34.5, 60.2, and 62.4°2θ could be assigned to the (003), (006), (009), (110), and (113) reflections of LDH, respectively, characteristic of a layered structure (Ferreira et al. 2004; Carvalho et al. 2015). They were consistent with the standard card JCPDS 40-0216. Almost identical, typical structures were observed in the XRD patterns of the MgAlLa-0.2-L, MgAlLa-0.4-L, and MgAlLa-0.5-L precursors. Compared with MgAl-L, they had the characteristics of a layered structure. Besides, the diffraction peaks at 15.5, 27.3, 27.9, 39.4, and 48.6°2θ could be indexed to $La(OH)_3$ (JCPDS 36-1481). In other words, when the initial La(III) molar ratio was in the range 0.2 to 0.5, $La(OH)_3$ and LDHs coexisted in MgAlLa-L.

However, the characteristic diffraction peak of hydrotalcite did not appear in MgAlLa-0.8-L and MgLa-1-L, indicating that the materials synthesized were not hydrotalcite when the Al(III)/La(III) molar ratio was 0.2:0.8 or when Al(III) was completely replaced by La(III). Besides the diffraction peak of $La(OH)_3$, the reflections at 18.4, 38.0, 50.8, and 58.6°2θ could be indexed to $Mg(OH)_2$ (JCPDS 44-1482), revealing the co-existence of $La(OH)_3$ and $Mg(OH)_2$ in MgLa-L.

The XRD patterns of MgAlLa-*x*-L calcined at 600°C (Fig. 2) revealed that the reflections corresponding to LDHs had disappeared completely and new reflections had appeared after calcination of MgAlLa-LDHs. The reflections at 42.8 and 62.3°2θ could be indexed to MgO (JCPDS No. 45-0946), whereas those at 31.3, 36.8, 44.8, 59.4, and 65.2°2θ could be indexed to $MgAl_2O_4$ (JCPDS No.21-1152). The $MgAl_2O_4$ spinel formed during the calcination process, similar to the work of Ahmed et al. (2012). With an increased La(III) content, the reflections at 26.1, 29.9, 39.5, 46.0, 52.1, and 55.4°2θ could be indexed to La_2O_3 (JCPDS No. 05-0602), whereas those at 11.4, 18.3, 27.6, 29.3, 33.4, 45.6, and 47.1°2θ could be indexed to $La_{10}Al_4O_{21}$ (JCPDS No.39-0009). The $La_{10}Al_4O_{21}$ spinel occurred at MgAlLa-0.4-M. These results may be ascribed to the homogeneous distribution of metal

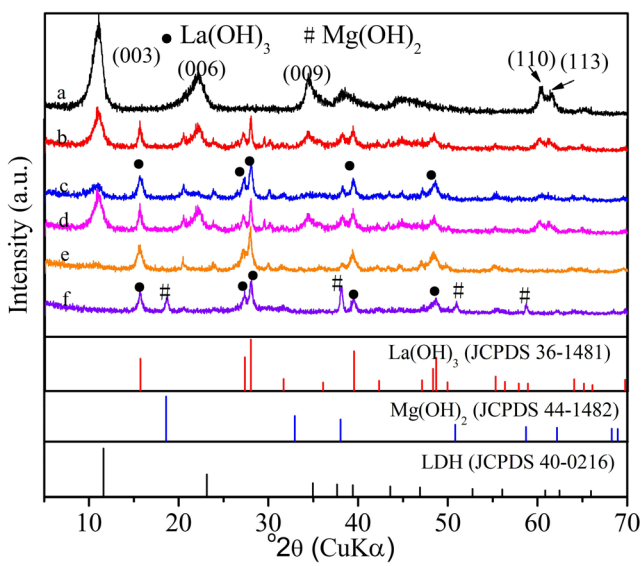

Fig. 1 XRD patterns of MgAlLa-L precursors: (**a**) MgAl-L, (**b**) MgAlLa-0.2-L, (**c**) MgAlLa-0.4-L, (**d**) MgAlLa-0.5-L, (**e**) MgAlLa-0.8-L, and (**f**) MgLa-1-L.

https://doi.org/10.1007/s42860-019-00023-2 Published online by Cambridge University Press

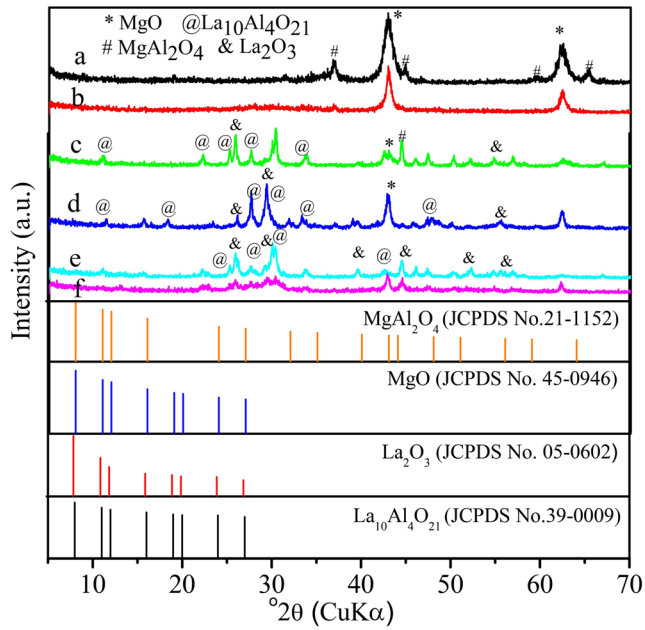

Fig. 2 XRD patterns of MgAlLa-M: (**a**) MgAl-M, (**b**) MgAlLa-0.2-M, (**c**) MgAlLa-0.4-M, (**d**) MgAlLa-0.5-M, (**e**) MgAlLa-0.8-M, and (**f**) MgLa-1-M.

ions within MgAlLa-LDHs, which facilitated the formation of well dispersed and crystalline mixed-metal oxides through a topotactic process during calcination (Zhao et al. 2010). No signal corresponding to an Al_2O_3 phase was detected, implying that the Al_2O_3 was amorphous. This was because, following the collapse of the MgAlLa-LDHs layered structure upon calcination, generation of MgO (La_2O_3) and Al_2O_3 subsequently gave rise to the formation of spinel, $MgAl_2O_4$ ($La_{10}Al_4O_{21}$) (Zhao et al. 2010).

FTIR spectroscopy analysis

The FTIR spectra of as-synthesized LDH samples (Fig. 3) were very similar to those reported generally for hydrotalcite-like compounds. The absorption peak between 3470 and ~3640 cm ^{1} in the IR spectra was ascribed to the stretching vibration of the OH group with hydrogen bonding from interlayer water molecules (Yan et al. 2015). Similarly, the band observed at 1630 cm^{-1} was attributed to the bending mode of crystalline water. An absorption peak at 1368 cm ^{1} was attributed to the telescopic vibration peak of NO_3^- (Scavetta et al. 2012). The bands at ~846 and 602 cm^{-1} arose from the metal-oxygen bonds (M-O, M-O-M, and M-OH) vibration in the LDHs. In the case of MgAlLa-0.4-L, MgAlLa-0.5-L, MgAlLa-0.8-L, and MgLa-1-L, a new band was observed at 3603 cm^{-1}, which corresponded to non-bonded OH group vibrations for $La(OH)_3$. An absorption peak at 3696 cm^{-1}

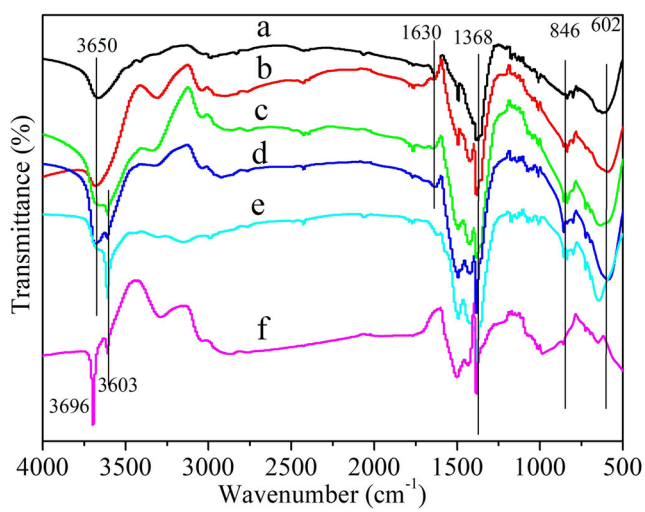

Fig. 3 FTIR spectra of MgAlLa-L precursors: (**a**) MgAl-L, (**b**) MgAlLa-0.2-L, (**c**) MgAlLa-0.4-L, (**d**) MgAlLa-0.5-L, (**e**) MgAlLa-0.8-L, and (**f**) MgLa-1-L.

https://doi.org/10.1007/s42860-019-00023-2 Published online by Cambridge University Press

corresponds to non-bonded OH group vibrations for $Mg(OH)_2$. Compared with uncalcined samples, the differences in infrared spectra might be due to the structural difference in compounds formed with different amounts of La. The above results were consistent with XRD analysis.

Morphology

The morphology of the MgAlLa-L with various molar ratios before calcination was characterized using SEM (Fig. 4). The MgAl-L synthesized showed many wrinkles on the surface (Fig. 4A1). MgAlLa-0.2-L and MgAlLa-0.4-L also displayed wrinkles on the surface (Fig. 4A2 and A3). Some fragments of MgAlLa-0.4-L also appeared. The morphology of MgAlLa-0.5-L (Fig. 4A4) changed significantly, and many irregular sheets aggregated. Needle-like and granular aggregates appeared for MgAlLa-0.8-L (Fig. 4A5) and MgLa-L (Fig. 4A6). With the increase in La(III) content in MgAlLa-L, the morphologies of the synthesized samples varied greatly.

The morphology of the MgAlLa-M with various molar ratios (Fig. 5) showed that MgAl-M after calcination was made up of irregular, multilateral sheets and some particles. In contrast, the multilateral fragments on the surface of MgAlLa-0.2-M and MgAlLa-0.4-M were more obvious (Fig. 5B2 and B3). The morphology of MgAlLa-0.5-M collapsed from a specific structure and became regular, agglomerated platelet-like particles after calcination at 600°C; the platelets had a side length of 0.08 μm (Fig. 5B4). Fine particles appeared for MgAlLa-0.8-M (Fig. 5B5) and MgLa-M (Fig. 5B6). The change in morphology seemed to be the result of MgAlLa-M having a large specific surface area. The EDX pattern (Fig. 5B7) further confirmed the presence of Mg, Al, La, and O in MgAlLa-0.5-M (Fig. 4F); the Mg(II)/Al(III)/La(III) molar ratio was close to 3:0.5:0.5.

Optical properties

The UV-Vis absorption spectra of the as-prepared samples (Fig. 6A and C) revealed that the MgAlLa-M had a better absorbance stability than MgAlLa-L, and the absorption edge was extended to ~800 nm covering the full visible light spectrum, compared with the absorption edges of MgAlLa-L. The band-gap energies of the samples before and after calcination were calculated using the onset of the UV Vis spectra of the absorption values (Eq. 1) (Hussain et al., 2011)

$$(a\mathrm{h}\nu)^2 = \mathrm{K}(\mathrm{h}\nu - Eg) \quad (1)$$

Where a is the absorption coefficient, ν represents the light frequency, Eg is the band gap energy, K is a proportionality constant, and h is Planck s constant. The normalized graphs of $(a\mathrm{h}\nu)^2$ for the photon energy of the MgAlLa-L and MgAlLa-M samples (Fig. 6B and D) showed that all MgAlLa-M samples exhibited relatively lower band gap energy and were expected to show better photocatalytic activity compared with MgAlLa-L. The smaller band-gap might be attributed to the composite oxides formed by calcination, and the band-gap values of MgAlLa-M samples (3.11 3.35 eV) were smaller than those of MgAl-M (3.36 eV). The MgAlLa-M samples were thus expected to show better photocatalytic activity than MgAl-M under visible light. This result could be attributed to the coupling interaction among the MgO, La_2O_3, $MgAl_2O_4$, and $La_{10}Al_4O_{21}$ phases, the optimizing content of MgO, La_2O_3, and the form of heterojunction structure, which led to the enhancement of utilization of light and photocatalytic activity (Zhang et al., 2016).

Influence of light

The influence of light on the photocatalytic activity of MgAlLa-0.5-M was determined by degradation of MB (Fig. 7). The residual amount of MB was almost unchanged with no light, which indicated that the adsorption of MB by MgAlLa-0.5-M was weak. Another test without light demonstrated that MB could not be degraded under MgAlLa-0.5-M/H_2O_2, because the residual level of MB was 91.65% after reaction for 60 min. When the MB solutions were light irradiated for 60 min, however, the residual MB was only 0.11% under MgAlLa-0.5-M/H_2O_2. Meanwhile, the color of the MB

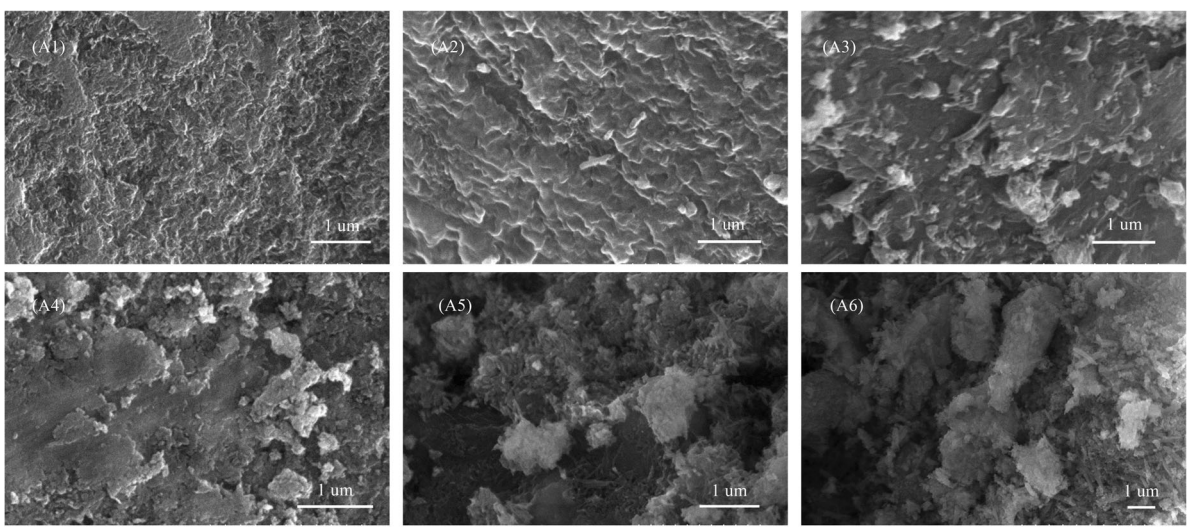

Fig. 4 SEM images of MgAl-L (A1), MgAlLa-0.2-L (A2), MgAlLa-0.4-L (A3), MgAlLa-0.5-L (A4), MgAlLa-0.8-L (A5), and MgLa-L (A6).

https://doi.org/10.1007/s42860-019-00023-2 Published online by Cambridge University Press

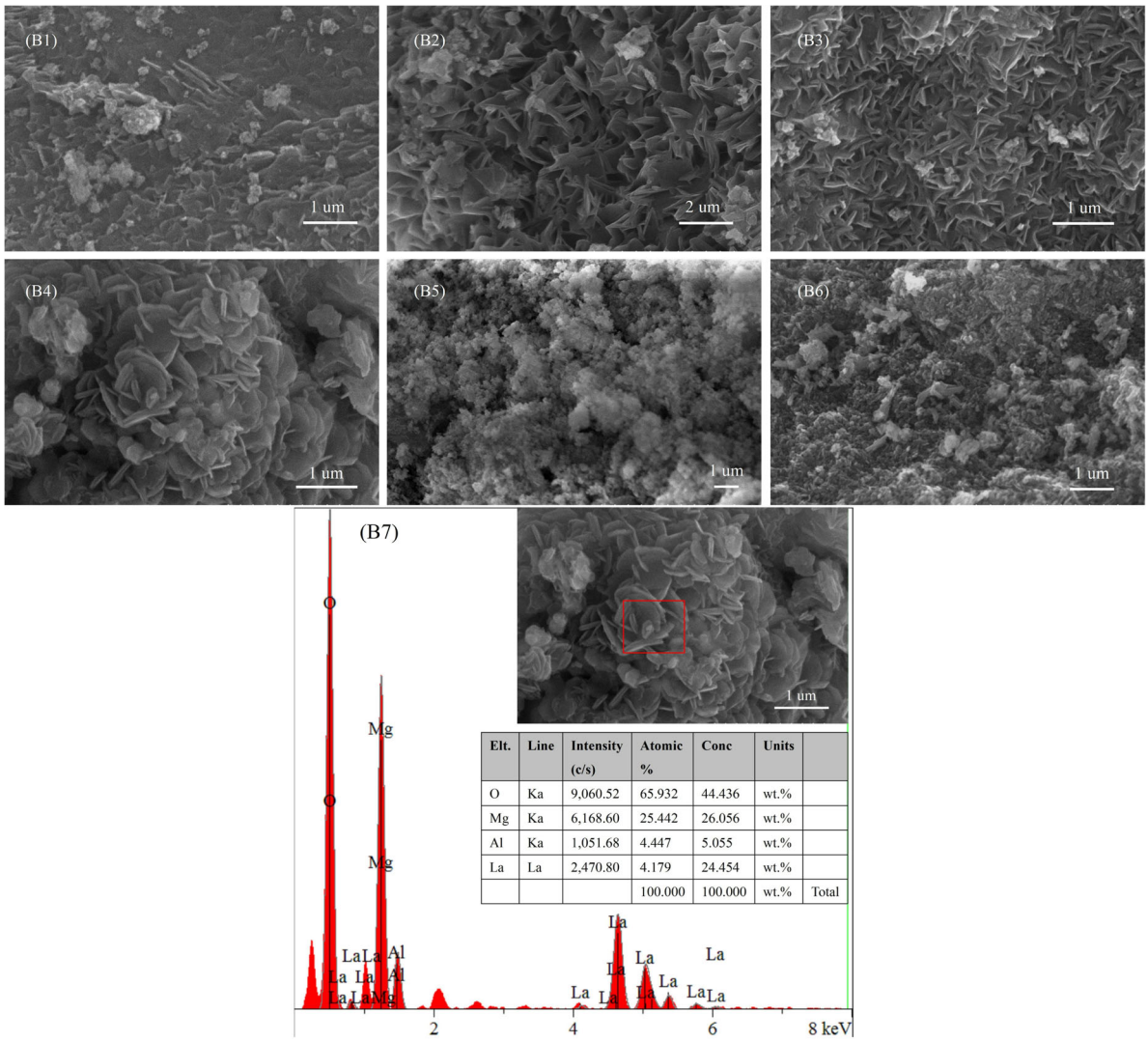

Elt.	Line	Intensity (c/s)	Atomic %	Conc	Units	
O	Ka	9,060.52	65.932	44.436	wt.%	
Mg	Ka	6,168.60	25.442	26.056	wt.%	
Al	Ka	1,051.68	4.447	5.055	wt.%	
La	La	2,470.80	4.179	24.454	wt.%	
			100.000	100.000	wt.%	Total

Fig. 5 SEM images of MgAl-M (B1), MgAlLa-0.2-M (B2), MgAlLa-0.4-M (B3), MgAlLa-0.5-M (B4), MgAlLa-0.8-M (B5), and MgLa-M (B6), along with EDX measurement of MgAlLa-0.5-M (B7).

solution was close to colorless, which led to the conclusion that photocatalytic degradation of MB in the MgAlLa-0.5-M and H_2O_2 system is accelerated by light irradiation.

Effect of catalyst

Under illumination only, the residual amount of MB was 84% after 1 h, and the rate of degradation was very slow (Fig. 8). When 0.5 mL H_2O_2 was added, the degradation rate of MB increased, and the residual amount was 70.1% after 1 h. The photocatalytic degradation efficiency of MB with 50 mg of MgAl-M was almost the same as that by MB only. The degradation efficiency of MgAlLa-0.5-M was more obvious, and the residual MB was 36.23% after 60 min. The degradation rate of MB increased significantly when the catalyst and H_2O_2 acted simultaneously. The results above showed that the catalytic degradation of MB by a single catalyst was not ideal, only when MgAlLa-M and H_2O_2 were used in concert was the best level of photocatalytic degradation achieved; photocatalytic degradation efficiency of MB dye with MgAlLa-0.5-M under visible light irradiation for 1 h was 99.89%, which exceeded the binary MgAl-M (84.06%) under the same conditions. This might be attributed to the introduction of La(III) to improve the photocatalytic activity of mixed-metal oxides.

Effect of MgAlLa-L/H_2O_2

The photocatalytic effect of MgAlLa-L with a molar ratio of Mg(II)/Al(III)/La(III) (Fig. 9) showed that MgAlLa-L possessing different molar ratios exhibited a strong catalytic degradation ability for MB, and that the La(III) content affected the photocatalytic degradation rate. The photocatalytic effect of MgAlLa-L/H_2O_2 increased when the La(III) content decreased. When Al(III) was completely replaced by La(III),

https://doi.org/10.1007/s42860-019-00023-2 Published online by Cambridge University Press

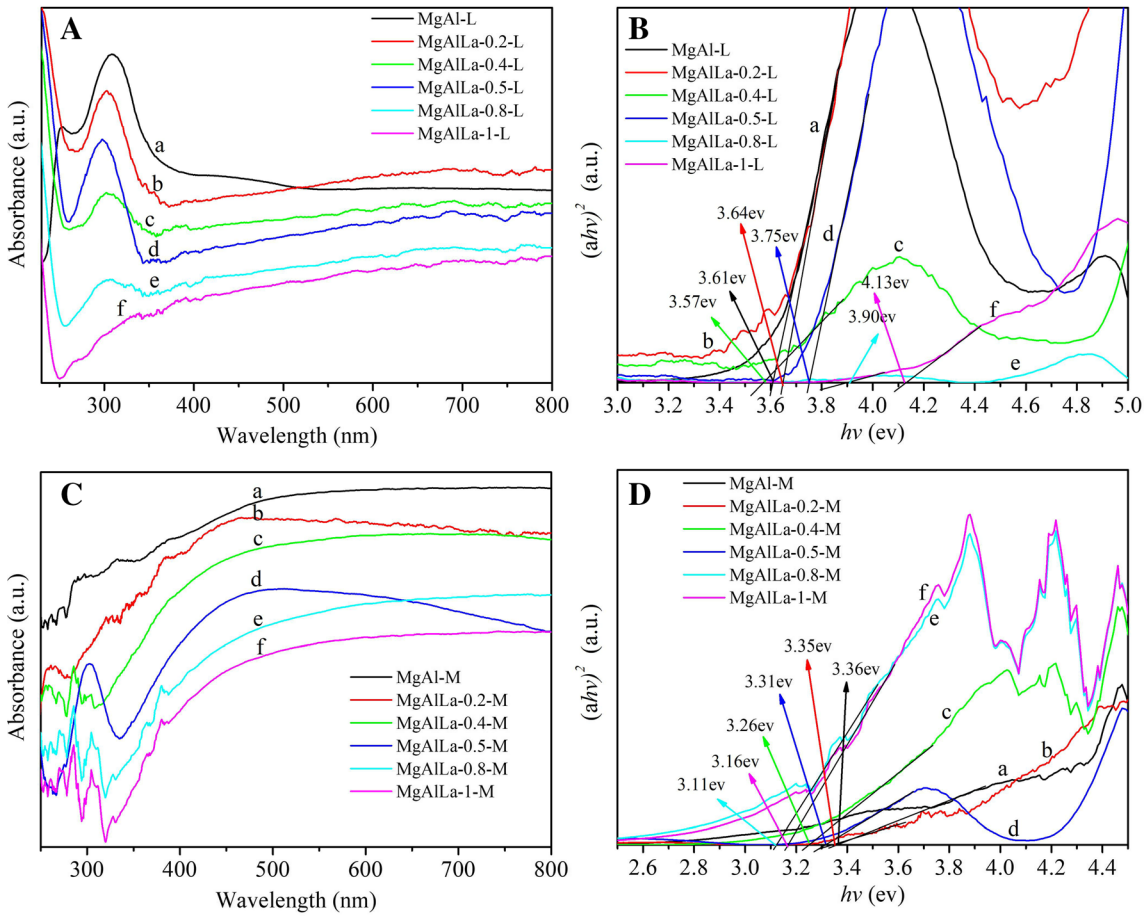

Fig. 6 UV-Vis absorption spectra of the MgAlLa-L (**A**) and MgAlLa-M (**C**), and the plotting of $(ah\nu)^2$ vs. $h\nu$ based on the direct transition (**B**, **D**). MgAlLa-L (**A**, **B**): (a) MgAl-L, (b) MgAlLa-0.2-L, (c) MgAlLa-0.4-L, (d) MgAlLa-0.5-L, (e) MgAlLa-0.8-L, and (f) MgLa-1-L. MgAlLa-M (**B**, **D**): (a) MgAl-M, (b) MgAlLa-0.2-M, (c) MgAlLa-0.4-M, (d) MgAlLa-0.5-M, (e) MgAlLa-0.8-M, and (f) MgLa-1-M.

however, the photocatalytic activity was best. According to XRD analysis, MgLa-1-L does not have a hydrotalcite structure, so the basic substances such as $Mg(OH)_2$ and $La(OH)_3$ in the MgLa-1-L possibly played a photocatalytic role.

Effect of MgAlLa-M/H_2O_2

The photocatalytic effect of La_2O_3 on MB (Fig. 10) was not obvious; after 60 min the residual MB was >60% (contrast

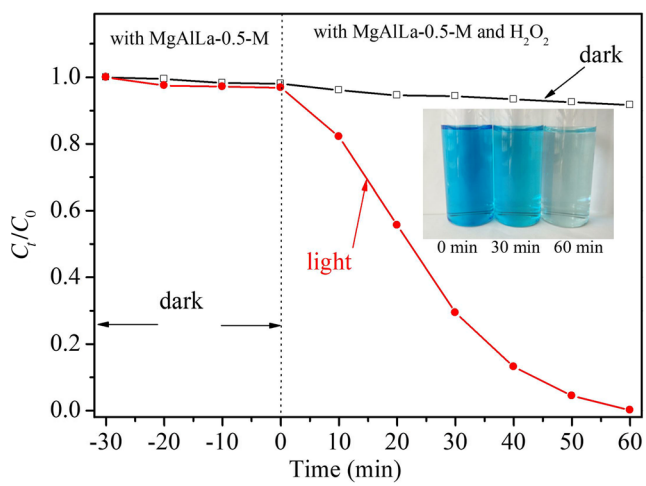

Fig. 7 Effect of light on photocatalytic degradation of MB with MgAlLa-0.5-M.

https://doi.org/10.1007/s42860-019-00023-2 Published online by Cambridge University Press

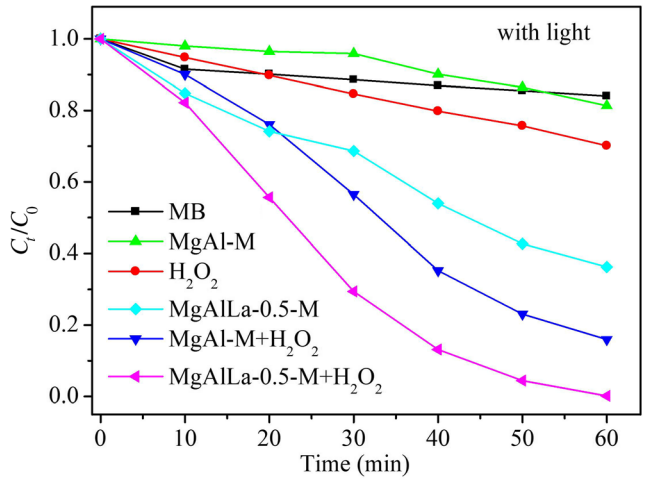

Fig. 8 Effect of catalyst on photocatalytic degradation of MB.

experiment), which indicated that La_2O_3 did not play a major role in the photocatalytic process. When Mg-Al hydrotalcite was calcined to form mixed-metal oxides, the residual MB was 15.9% after photocatalytic degradation for 60 min. While Mg(II), Al(III), and La(III) coexisted in the composite oxides (the molar ratio of La(III) being from 0.2 to 0.8), the MB residue decreased and the catalytic activity of MgAlLa-M increased. When the molar ratio of Mg(II):Al(III):La(III) was 3:0.5:0.5, the photocatalytic activity of MgAlLa-0.5-M was better than that of MgAl-M and the residual MB was only 0.11% after 60 min. The photocatalytic MB effect of the mixed-metal oxides that formed when Al(III) was replaced completely by La(III) was most obvious, and the degradation was completed within 30 min. Irradiation at ~150 W from a halogen lamp was less bright than with a xenon lamp. In addition, the reaction time was 30 60 min, which shortened the illumination time and improved the photocatalytic efficiency.

The catalytic activity of MgAlLa-M for MB was obviously better than that of MgAlLa-L (Fig. 11). This was because the mixed-metal oxides contain MgO, La_2O_3, $MgAl_2O_4$, and $La_{10}Al_4O_{21}$, which had a relatively smaller band gap than MgAlLa-L, thereby improving the visible light absorption of the mixed-metal oxides. On the other hand, the effects of photocatalytic degradation of MB by MgAlLa-L or MgAlLa-M was irregular as the La content increased, which might be related to the composition and morphology of the composite oxides.

The interface heterostructures in MgAlLa-M were different. Heterojunctions with good electron (e) and hole (h^+) transport channels could be formed at the interface of MgAlLa-M with appropriate molar ratios of Mg(II), Al(III), and La(III). Moreover, the key factor of high photocatalytic activity was the effective separation of photogenerated e^- and h^+ pairs. Consequently, when the molar ratio of Mg(II), Al(III), and La(III) was appropriate in MgAlLa-M, MgAlLa-M displayed excellent photocatalytic performance. The photocatalytic activity of MgAlLa-0.5-M on MB was slightly better than that of MgLa-1-M, and the photocatalytic performance of MgAlLa-M was better than that of MgAl-M, inferring that hydrotalcite-based mixed-metal oxides prepared with MgAl-LDHs as precursors, which added La(III), improves the

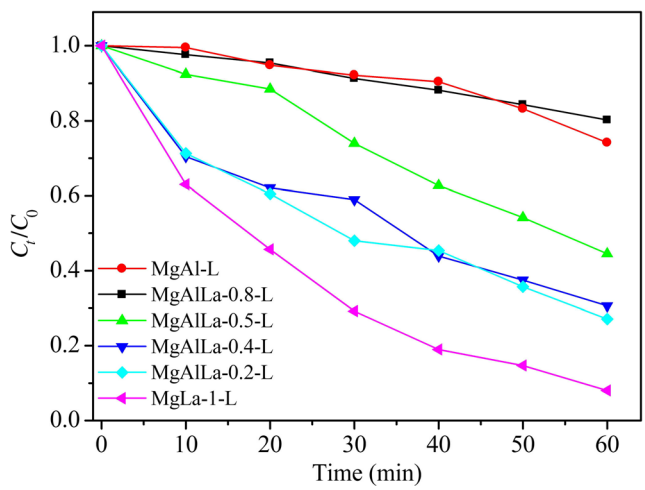

Fig. 9 Photocatalytic degradation of MB with MgAlLa-L/H_2O_2.

https://doi.org/10.1007/s42860-019-00023-2 Published online by Cambridge University Press

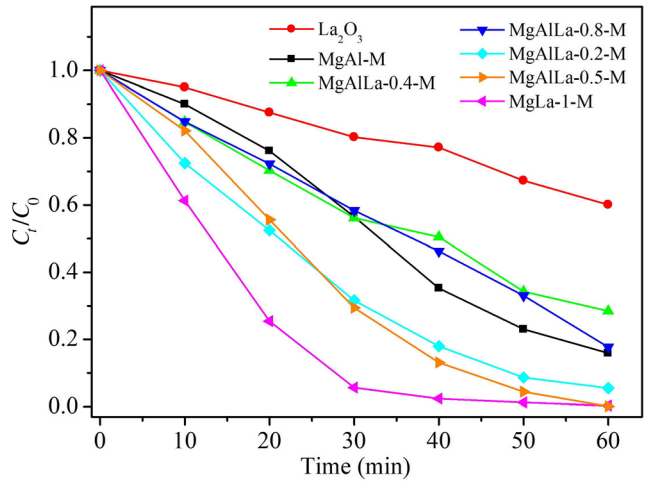

Fig. 10 Photocatalytic degradation of MB with MgAlLa-M/H_2O_2.

degradation ability of the catalyst toward MB. Interestingly, in contrast with MgLa-0.5-M, MgLa-1-M had a higher ratio of La(III) but showed no improvement in photocatalytic activity, suggesting that the amount of La(III) was the crucial factor.

UV-Vis absorption spectra of MB

The UV-Vis absorption spectra (Fig. 12) showed a strong absorption peak at 664 nm which belonged mainly to the conjugated system of aromatic rings in the MB structure. With the prolongation of photocatalytic reaction time, the maximum absorption peak of MB solution weakened gradually. This was due to the destruction of display groups, which consist of chromophore and cochromophore in MB during the photocatalytic reaction. When photocatalysis lasted for 60 min, the absorption peak was no longer obvious, which was attributed to the interruption of the unsaturated conjugate bond of the chromophore group during the photocatalytic degradation of MB.

Photocatalytic mechanism

To further elucidate the reaction mechanism, the reactive species were determined in the presence of isopropanol (IPA), *p*-benzoquinone (BQN), and disodium ethylenediamine tetraacetic acid (EDTA) as scavengers of hydroxyl radicals (OH), superoxide radicals (O_2), and photoexcited holes (h^+), respectively (Yan et al. 2013). So, in the reaction system, the mole ratio of MB to the capture agent was 1:200.

When the MB solutions (Fig. 13) were irradiated for 60 min, the residual amounts of MB were 33.78%, 10.63%, and 2.92% over BQN, EDTA, and IPA, respectively. A significant decrease of photocatalytic performance in the presence of BQN was observed, implying that O^2 played a major role in the photocatalytic reaction. Moreover, the photocatalytic performance decreased slightly in the presence of IPA and EDTA, suggesting that the OH and h^+ were the less important reactive species for the decomposition of MB.

The possible mechanism of photocatalytic degradation of MB is as follows. Photo-induced e^-/h^+ pairs were generated on

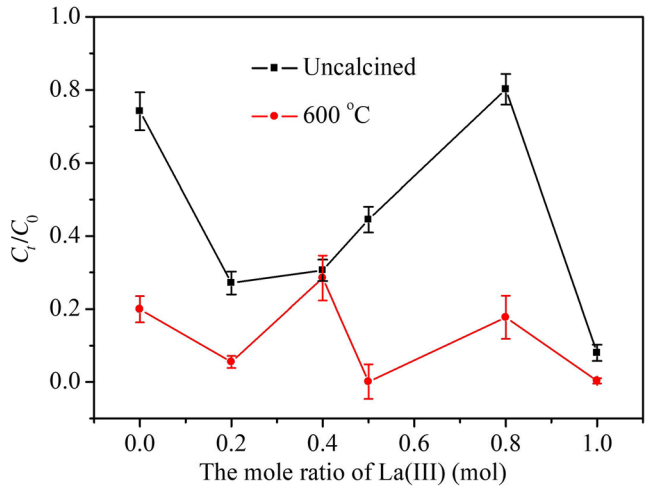

Fig. 11 Comparison of photocatalytic activity of MgAlLa-L and MgAlLa-M with various La(III) contents.

https://doi.org/10.1007/s42860-019-00023-2 Published online by Cambridge University Press

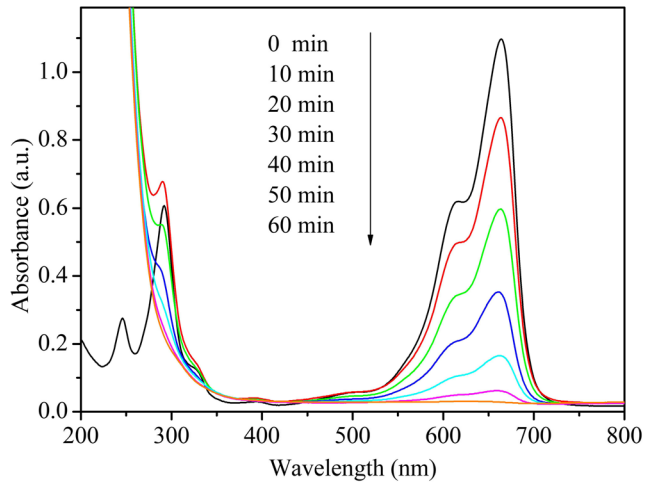

Fig. 12 The UV-Vis absorption spectra of MB with MgAlLa-0.5-M/H_2O_2.

the surface of the photocatalyst MgAlLa-M during irradiation (Eq. 1). The photoinduced h^+-oxidized H_2O_2 molecules that were adsorbed on the photocatalyst surface into OH species (Eq. 2), while the photoinduced e^--activated H_2O_2 and O_2 molecules adsorbed on the catalyst surface into OH, OH^- species (Eq. 3) and O_2^- species (Eq. 4), respectively. In addition, OH species were also generated during irradiation of H_2O_2 (Eq. 5). H_2O_2 oxidized the active O_2^- species into OH, OH^-, and O_2 species (equation 6). The OH and O_2 are the main active species in the photocatalytic reaction (Ishibashi et al. 2000; Liu & Sun 2011; Xiang et al. 2011). The MB molecules were oxidized by OH and O_2 species into small molecules (Eqs. 7 and 8).

$$\mathrm{MgAlLa{-}M} + \mathrm{h}v \rightarrow e + h^+ \quad (2)$$

$$h^+ + \mathrm{H_2O_2} \rightarrow 2\ \mathrm{OH} \quad (3)$$

$$e + \mathrm{H_2O_2} \rightarrow \mathrm{OH} + \mathrm{OH} \quad (4)$$

$$e + \mathrm{O_2} \rightarrow \mathrm{O_2} \quad (5)$$

$$H_2O_2 + \mathrm{h}v \rightarrow 2\ \mathrm{OH} \quad (6)$$

$$\mathrm{O_2} + \mathrm{H_2O_2} \rightarrow \mathrm{OH} + \mathrm{OH} + \mathrm{O_2} \quad (7)$$

$$\mathrm{OH} + \mathrm{MB} \rightarrow \text{Degradation products} \quad (8)$$

$$\mathrm{O_2} + \mathrm{MB} \rightarrow \text{Degradation products} \quad (9)$$

Based on the above discussions and the experimental results of MB degradation under different capture agents, when BQN was added to the reaction system, the O_2^- was captured, so reactions 6, 7, and 8 were hindered, which would hinder the degradation process of MB. On the other hand, reaction 4 proceeded to the right while trapping O_2^-. As a result, the formation of h^+ and OH was accelerated. But the degradation of MB had not accelerated, implying that O_2^- played a major role in the photocatalytic reaction.

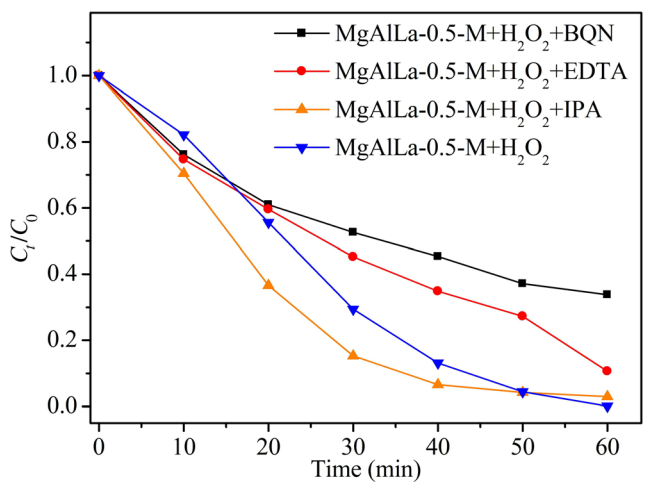

Fig. 13 Active species trapping experiments under visible light irradiation.

https://doi.org/10.1007/s42860-019-00023-2 Published online by Cambridge University Press

When EDTA was added, the h^+ was captured, and reaction 2 was hindered and the amount of OH produced was reduced, which would diminish the degradation of MB. Although the h^+ was captured, reaction 1 was pushed to the right, which led to the production of a large amount of e^- at the surface and inside the catalyst. The production of e^- and H_2O_2 and O_2 in the solution is enabled by reactions 3 and 4 to produce OH and O_2^-. The OH could effectively oxidize MB, while O_2^- and H_2O_2 could react according to reaction 6 to produce OH and O_2, which could oxidize MB (Liu & Sun 2011). The experimental results showed, however, that the degradation of MB slows down after adding EDTA, so one could speculate that reaction 2 was the key step in the degradation of MB.

In addition, when IPA was present, OH in the solution was captured, which hindered the progress of reaction 7, but enabled reactions 2, 3, and 6 to proceed to the right. At the same time, reaction 1 was accelerated. A large number of e^- and h^+ were produced in the solution, which accelerated the formation of O_2 and promoted the degradation of MB. In fact, in the photocatalytic degradation of MB, many bubbles were produced in the solution, leading to speculation that MB was degraded according to reaction 8. This was consistent with the results of accelerating the degradation of MB under isopropanol.

Based on the aforementioned experimental results, a possible mechanism for the enhanced photoactivity of MgAlLa-0.5-M/H_2O_2 is proposed. Under visible-light irradiation, photogenerated e^- and h^+ is formed at the inside of MgAlLa-M after irradiation. These e^- and h^+ move freely within the MgAlLa-M. When they move to the surface, e^- interacts with O_2 and H_2O_2 in the solution to form O_2 and OH, and h^+ reacts with H_2O_2 to form OH, which together promotes the oxidative decomposition of MB. In addition, in the reaction system of MgAlLa-0.5-M/H_2O_2, O_2^- plays a major role and the h^+ and OH are the less important reactive species for the decomposition of MB.

CONCLUSIONS

In this work, ternary MgAlLa mixed-metal oxides (MgAlLa-M) were synthesized via a hydrotalcite-like precursor route. Analysis by XRD showed that MgO, La_2O_3, $MgAl_2O_4$, and $La_{10}Al_4O_{21}$ phases coexisted in calcined samples as MgAlLa-M. MgAlLa-M had a smaller band gap and stronger visible light absorption ability than binary MgAl mixed-metal oxides. The photocatalytic degradation efficiency of MB dye with MgAlLa-0.5-M under visible light irradiation for 1 h was 99.89% in the presence of H_2O_2, which exceeded binary MgAl-M (84.06%) under the same conditions. The high photocatalytic activity of the sample was attributed to the addition of La(III). The high activity radicals of O_2^- played a major role.

ACKNOWLEDGEMENTS

This work was supported financially by the Zhejiang Provincial Natural Science Foundation of China (LQ19E040001 and LY14B060006).

REFERENCES

Ahmed, A. A. A., Talib, Z. A., Hussein, M. Z. B., & Zakaria, A. (2012). Improvement of the crystallinity and photocatalytic property of zinc oxide as calcination product of Zn Al layered double hydroxide. *Journal of Alloys and Compounds, 539*, 154 160. https://doi.org/10.1016/j.jallcom.2012.05.093.

Baliarsingh, N., Mohapatra, L., & Parida, K. (2013). Design and development of a visible light harvesting Ni Zn/Cr CO_3^{2} LDH system for hydrogen evolution. *Journal of Materials Chemistry A, 13*, 4236 4243. https://doi.org/10.1039/C2TA00933A.

Carvalho, D. C., Ferreira, N. A., Filho, J. M., Ferreira, O. P., Soares, J. M., & Oliveira, A. C. (2015). Ni Fe and Co Fe binary oxides derived from layered double hydroxides and their catalytic evaluation for hydrogen production. *Catalysis Today, 250*, 155 165. https://doi.org/10.1016/j.cattod.2014.08.010.

Carja, G., Dartu, L., Okada, K., & Fortunato, E. (2013). Nanoparticles of copper oxide on layered double hydroxides and the derived solid solutions as wide spectrum active nano-photocatalysts. *Chemical Engineering Journal, 222*, 60 66. https://doi.org/10.1016/j.cej.2013.02.039.

Chen, Y., Zhou, S., Li, F., Wei, J., Dai, Y., & Chen, Y. (2011). Fluorescence and phase transitions of Mg-Al-Eu ternary layered double hydroxides-dependence on annealing. *Clay Minerals, 46*, 487 493. https://doi.org/10.1007/s10895-011-0857-8.

Chen, J., Lei, Z., Wang, A., Liu, J., Wu, X., Chang, T., Zhang, Y., & Li, M. (2015). Structure analysis and fluorescence of Mg-Al-Tb ternary layered double hydroxides and their calcined products. *Journal of Metals, 67*, 354 360. https://doi.org/10.1007/s11837-014-1210-x.

Curtius, H., & Ufer, K. (2007). Eu incorporation behavior of a Mg-Al-Cl layered double hydroxide. *Clays and Clay Minerals, 55*, 354 360. https://doi.org/10.1346/ccmn.2007.0550403.

Fan, G., Sun, W., Wang, H., & Li, F. (2011). Visible-light-induced heterostructured Zn Al In mixed metal oxide nanocomposite photocatalysts derived from a single precursor. *Chemical Engineering Journal, 174*, 467 474. https://doi.org/10.1016/j.cej.2011.09.054.

Ferreira, O. P., Alves, O. L., Gouveia, D. X., Filho, A. G. S., Paiva, J. A. C. D., & Filho, J. M. (2004). Thermal decomposition and structural reconstruction effect on Mg Fe-based hydrotalcite compounds. *Journal of Solid State Chemistry, 177*, 3058 3069. https://doi.org/10.1016/j.jssc.2004.04.030.

Heredia, A. C., Oliva, M. I., Agú, U., Zandalazini, C. I., Marchetti, S. G., Herrero, E. R., & Crivello, M. E. (2013). Synthesis, characterization and magnetic behavior of Mg Fe Al mixed oxides based on layered double hydroxide. *Journal of Magnetism and Magnetic Materials, 342*, 38 46. https://doi.org/10.1016/j.jmmm.2013.04.057.

Hussain, M., Russo, N., & Saracco, G. (2011). Photocatalytic abatement of VOCs by novel optimized TiO_2 nanoparticles. *Chemical Engineering Journal, 166*, 138 149. https://doi.org/10.1016/j.cej.2010.10.040.

Ishibashi, K. I., Fujishima, A., Watanabe, T., & Hashimoto, K. (2000). Quantum yields of active oxidative species formed on TiO_2 photocatalyst. *Journal of Photochemistry and Photobiology A-Chemistry, 134*, 139 142. https://doi.org/10.1016/S1010-6030(00)00264-1.

Kong, Y., Li, Y., Hu, G., Jing, L., Pan, D., Dong, D., et al. (2018). Preparation of polystyrene-b-poly(ethylene/propylene)-b-polystyrene grafted glycidyl methacrylate and its compatibility with recycled polypropylene/recycled high impact polystyrene blends. *Polymer, 145*, 232 241. https://doi.org/10.1016/j.polymer.2018.05.017.

Lan, M., Fan, G., Yang, L., & Li, F. (2014). Enhanced visible-light-induced photocatalytic performance of a novel ternary semiconductor coupling system based on hybrid Zn In mixed metal oxide/g-C3N4 composites. *RSC Advances, 5*, 5725 5734. https://doi.org/10.1039/C4RA07073A.

Li, S. D., Wang, H. S., Li, W. M., Wu, X. F., Tang, W. X., & Chen, Y. F. (2015). Effect of Cu substitution on promoted benzene oxidation

over porous CuCo-based catalysts derived from layered double hydroxide with resistance of water vapor. *Applied Catalysis B Environmental, 166-167*, 260 269. https://doi.org/10.1016/j.apcatb.2014.11.040.

Li, Y., Wu, X., Song, J., Li, J., Shao, Q., Cao, N., et al. (2017). Reparation of recycled acrylonitrile- butadiene-styrene by pyromellitic dianhydride: reparation performance evaluation and property analysis. *Polymer, 124*, 41 47. https://doi.org/10.1016/j.polymer.2017.07.042.

Liu, N., & Sun, G. (2011). Photo-degradation of methylene blue in the presence of 2-anthraquinone sulfonate and cyclohexanol presence. *Dyes and Pigments, 91*, 215 224. https://doi.org/10.1016/j.dyepig.2011.03.018.

Mao, N., Zhou, C. H., Tong, D. S., Yu, W. H., & Cynthia Lin, C. X. (2017). Exfoliation of layered double hydroxide solids into functional nanosheets. *Applied Clay Science, 144*, 60 78. https://doi.org/10.1016/j.clay.2017.04.021.

Muñoz, M., Moreno, S., & Molina, R. (2012). Synthesis of Ce and Pr-promoted Ni and Co catalysts from hydrotalcite type precursors by reconstruction method. *International Journal of Hydrogen Energy, 37*, 18827 18842. https://doi.org/10.1016/j.ijhydene.2012.09.132.

Nivangune, N. T., Ranade, V. V., & Kelkar, A. A. (2017). MgFeCe ternary layered double hydroxide as highly efficient and recyclable heterogeneous base catalyst for synthesis of dimethyl carbonate by transesterification. *Catalysis Letters, 147*, 2558 2569. https://doi.org/10.1007/s10562-017-2146-x.

Ömer, Ş., Kaya, M., & Saka, C. (2015). Plasma-surface modification on bentonite clay to improve the performance of adsorption of methylene blue. *Applied Clay Science, 116*, 46 53. https://doi.org/10.1016/j.clay.2015.08.015.

Özdemir, A., & Keskin, C. S. (2009). Removal of a binary dye mixture of congo red and malachite green from aqueous solutions using a bentonite adsorbent. *Clays and Clay Minerals, 57*, 695 705. https://doi.org/10.1346/CCMN.2009.0570603.

Pan, D., Ge, S., Zhao, J., Shao, Q., Guo, L., Zhang, X., et al. (2018). Synthesis, characterization and photocatalytic activity of mixed-metal oxides derived from NiCoFe ternary layered double hydroxides. *Dalton Transactions, 47*, 65 78. https://doi.org/10.1039/C8DT01045E.

Parida, K., Satpathy, M., & Mohapatra, L. (2012). Incorporation of $Fe^{(III)}$ into Mg/Al layered double hydroxide framework: effects on textural properties and photocatalytic activity for H_2 generation. *Journal of Materials Chemistry, 22*, 7350 7357. https://doi.org/10.1039/c2jm15658j.

Sahu, R. K., Mohanta, B. S., & Das, N. N. (2013). Synthesis, characterization and photocatalytic activity of mixed oxides derived from ZnAlTi ternary layered double hydroxides. *Journal of Physics and Chemistry of Solids, 74*, 1263 1270. https://doi.org/10.1016/j.jpcs.2013.04.002.

Scavetta, E., Ballarin, B., Corticelli, C., Gualandi, I., Tonelli, D., Prevot, V., Forano, C., & Mousty, C. (2012). An insight into the electrochemical behavior of Co/Al layered double hydroxide thin films prepared by electrodeposition. *Journal of Power Sources, 201*, 360 367. https://doi.org/10.1016/j.jpowsour.2011.10.122.

Shi, L., Li, D., Wang, J., Li, S., Evans, D. G., & Duan, X. (2005). Synthesis, flame-retardant and smoke-suppressant properties of a borate-intercalated layered double hydroxide. *Clays and Clay Minerals, 53*, 294 300. https://doi.org/10.1346/ccmn.2005.0530309.

Shu, X., He, J., Chen, D., & Wang, Y. (2008). Tailoring of phase composition and photoresponsive properties of Ti-containing nanocomposites from layered precursor. *The Journal of Physical Chemistry C, 112*, 4151 4158. https://doi.org/10.1021/jp711091m.

Subhan, M. A., Ahmed, T., & Uddin, N. (2015). Synthesis, structure, Pl and photocatalytic activities of $La_2O_2CO_3$·CeO_2·ZnO fabricated by co-precipitation method. *Spectrochimica Acta Part A Molecular and Biomolecular Spectroscopy, 138*, 827 833. https://doi.org/10.1016/j.saa.2014.10.114.

Wang, Z., Fongarland, P., Lu, G., & Essayem, N. (2014). Reconstructed La-, Y-, Ce-modified MgAl-hydrotalcite as a solid base catalyst for aldol condensation: investigation of water tolerance. *Journal of Catalysis, 318*, 108 118. https://doi.org/10.1016/j.jcat.2014.07.006.

Wu, W., Huang, Z. H., & Lim, T. T. (2014). Recent development of mixed metal oxide anodes for electrochemical oxidation of organic pollutants in water. *Applied Catalysis A: General, 480*, 58 78. https://doi.org/10.1016/j.apcata.2014.04.035.

Xiang, X., Hima, H. I., Wang, H., & Li, F. (2008). Facile synthesis and catalytic properties of nickel-based mixed-metal oxides with mesopore networks from a novel hybrid composite precursor. *Chemistry of Materials, 20*, 1173 1182. https://doi.org/10.1021/cm702072t.

Xiang, Q., Yu, J., & Wong, P. K. (2011). Quantitative characterization of hydroxyl radicals produced by various photocatalysts. *Journal of Colloid and Interface Science, 357*, 163 167. https://doi.org/10.1016/j.jcis.2011.01.093.

Xiang, X., Xie, L., Li, Z., & Li, F. (2013). Ternary MgO/ZnO/In_2O_3 heterostructured photocatalysts derived from a layered precursor and visible-light-induced photocatalytic activity. *Chemical Engineering Journal, 221*, 222 229. https://doi.org/10.1016/j.cej.2013.02.030.

Xu, M., Pan, G., Meng, Y., Guo, Y., Wu, T., & Chen, H. (2019). Effect of Ce^{3+} on the photocatalytic activity of MAlCe ternary hydrotalcites-like compounds in methylene blue photodegradation. *Applied Clay Science, 170*, 46 56. https://doi.org/10.1016/j.clay.2019.01.011.

Yan, T., Zhu, H., Li, R., Li, Z., Liu, J., & Wang, G. (2013). Microwave synthesis of nickel/cobalt double hydroxide ultrathin flowerclusters with three-dimensional structures for high-performance supercapacitors. *Electrochim Acta, 111*, 71 79. https://doi.org/10.1016/j.electacta.2013.07.215.

Yan, L., Yang, K., Shan, R., Yan, T., Wei, J., Yu, S., Yu, H., & Du, B. (2015). Kinetic, isotherm and thermodynamic investigations of phosphate adsorption onto core shell Fe_3O_4@ LDH composites with easy magnetic separation assistance. *Journal of Colloid and Interface Science, 448*, 508 516. https://doi.org/10.1016/j.jcis.2015.02.048.

Yang, R., Cui, Y., Yan, Q., Zhang, C., Qiu, L., O'Hare, D., & Wang, Q. (2017). Design of highly efficient NOx storage-reduction catalysts from layered double hydroxides for NOx emission control from naphtha cracker flue gases. *Chemical Engineering Journal, 326*, 656 666. https://doi.org/10.1016/j.cej.2017.06.016.

Zhao, X., Zhang, F., Xu, S., Evans, D. G., & Duan, X. (2010). From layered double hydroxides to ZnO-based mixed metal oxides by thermal decomposition: transformation mechanism and UV-blocking properties of the product. *Chemistry of Materials, 22*, 3933 3942. https://doi.org/10.1021/cm100383d.

Zhang, L., Dai, C. H., Zhang, X. X., Liu, Y. N., & Yan, J. H. (2016). Synthesis and highly efficient photocatalytic activity of mixed oxides derived from ZnNiAl layered double hydroxides. *Transactions of Nonferrous Metals Society of China, 26*, 2380 2389. https://doi.org/10.1016/S1003-6326(16)64360-1.

Zhou, C. H. (2010). Emerging trends and challenges in synthetic clay-based materials and layered double hydroxides. *Applied Clay Science, 48*, 1 4. https://doi.org/10.1016/j.clay.2009.12.018.

Zhou, C. H., & Keeling, J. (2013). Fundamental and applied research on clay minerals: from climate and environment to nanotechnology. *Applied Clay Science, 74*, 3 9. https://doi.org/10.1016/j.clay.2013.02.013.

Zhou, C. H., Li, Z. Z., Ai, Q. W., Tian, H. C., & Hong, P. H. (2016). Current fundamental and applied research into clay minerals in china. *Applied Clay Science, 119*, 3 7. https://doi.org/10.1016/j.clay.2015.07.043.

(Received 1 January 2019; revised 10 June 2019; AE: Chun-Hui Zhou)